Arch. Rational Mech. Anal. 131 (1995) 225–240.

Geometrical Aspects of Stability Theory for Hill's Equations

HENK BROER & MARK LEVI

Communicated by R. MCGEHEE

1. Introduction

There is by now a vast analytic theory of Mathieu's equation

$$\ddot{x} + (a + bp(t))x = 0, \quad p(t) \equiv p(t + 2\pi), \tag{1}$$

where a and b are real parameters. Apparently, the first stability diagram was drawn in the classical paper by B. VAN DER POL & M. J. O. STRUTT [15]. Since then many papers and textbooks have appeared on the subject; we mention J. J. STOKER [13], J. MEIXNER & F. W. SCHÄFKE [12], D. M. LEVY & J. B. KELLER [11], M. I. WEINSTEIN & J. B. KELLER [16, 17], J. PÖSCHEL & E. TRUBOWITZ [9] and V. I. ARNOLD [3, 5, 6]. This literature contains extensive estimates on the order of tangency of resonance tongues and the behavior of stability boundaries at infinity.

A full understanding of the stability diagrams is still lacking. For instance, the appearance of instability pockets in some cases (see Figure 1; cf. [15]) calls for a geometric explanation. It should be noted that this phenomenon does not occur in the classical Mathieu case; cf. [12]. For a preliminary study near resonances using singularity theory, we refer to AFSHARNEJAD [1]. Related bifurcational aspects of nonlinear perturbations of Mathieu's equation near resonances were studied by BROER & VEGTER [7]. The global geometry of the symplectic group was used for a stability proof of a Hill equation in LEVI [10].

We introduce the main object of study of this paper.

Definition 1. *Hill's map* is given by $H: (a, b) \mapsto P_{a,b}$, where $P_{a,b}$, is the Poincaré (or period) matrix of (1). Thus H maps $\mathscr{R}^2$ into $SP(1)$, the 3-dimensional space of symplectic 2×2-matrices.

Our driving motivation is to give a global geometric picture of Hill's map. This geometrical approach to this classical problem turns out to be very fruitful, giving a transparant explanation of the nature of the stability domains in the parameter plane.

Let us briefly describe our approach. Stability regions in the (a, b)-plane shown in Figure 1 are the preimages under Hill's map H of the stability domain in the

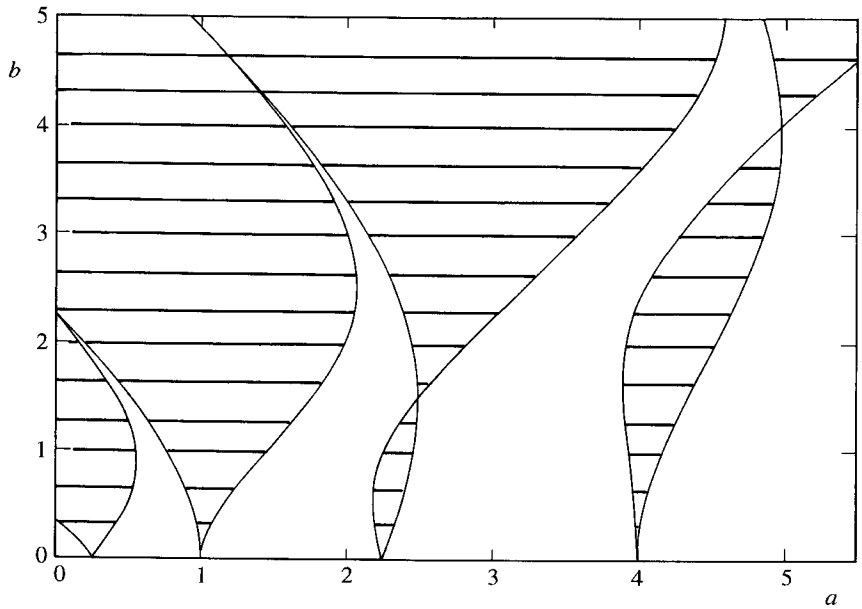

Figure 1. Stability diagram of Hill's equation when p is a square wave; cf. [15]. The diagram is symmetric with respect to the a-axis. Unstable regions are shaded.

symplectic group, Figure 3. The boundary of the stability domain in the neighborhood of $\pm I$ consists of a pair of cones, giving rise to the resonance tongues mentioned earlier. Restriction to the reversible case of even p (i.e., with $p(-t) \equiv p(t)$) reduces the range of H to a 2-dimensional cylinder inside the symplectic group; cf. Figure. 3. Our goal is to determine how H wraps and folds the (a, b)-plane around this cylinder.

The map H is studied by means of a decomposition $H = \pi \circ \Pi$, where $\Pi: \mathscr{R}^2 \to S$ is a diffeomorphism to a surface $S \subset \mathscr{R}^3$ and where π is a projection onto $\mathscr{R}^2$. The behavior of H now is completely described by the shape of S and in particular by the way in which π projects S. This approach is applied to two examples.

We conclude this introduction by summarizing our results. In Section 2 some facts about reversible symplectic 2×2 matrices are briefly reviewed.

In Section 3 we study a reversible deformation of the Mathieu equation at the second resonance $(a, b) = (1, 0)$, depending on a parameter ε. Local stability diagrams for $\varepsilon \approx 0$ are given in Figure 3. These diagrams can be geometrically understood by putting Hill's map $H = H_\varepsilon$ into a Whitney normal form, which is a 1-parameter family of folds. This naturally gives a decomposition $H = \pi \circ \Pi$; cf. Figure. 5. This approach, among other things, explains the following aspects of the stability diagrams in the Figure 3:

- For $\varepsilon = 0$ the boundaries have a nondegenerate tangency, which changes to a transversal crossing for $\varepsilon \neq 0$, thereby creating an instability pocket. This is explained by the fact that for $\varepsilon = 0$ the surface S folds (under the projection π)

above the matrix I; for $\varepsilon \neq 0$ the fold line moves away from I, which then is doubly covered by S in a diffeomorphic way.

- This geometry is persistent under C^2-small reversible perturbations of the family. Any L^p-small change of $q(t)$ in the class of even periodic functions leads to C^2-small perturbations of H.

In Section 4 we consider Hill's equation when p is a square wave: $\ddot{x} + (a + b \operatorname{sgn} \cos t)x = 0$. We explain the geometry of the whole stability diagram shown in Figure 1; cf. VAN DER POL & STRUTT [15]. Note that now the instability pockets have a more complicated combinatorial structure. Again we decompose Hill's map $H = \pi \circ \Pi$, with Π: $\mathscr{R}^2 \to S \subset \mathscr{R}^3$ a suitable diffeomorphism: see Figures 2 and 7. In order to keep track of all resonances $(a, b) = (\frac{1}{4}n^2, 0)$ we replace the cylinder of reversible symplectic matrices by its covering plane. The (shaded) instability domains antiproject to shaded regions of S which, in turn, are diffeomorphic to the instability domains in the (a, b)-plane. Here is a partial list of properties made transparent by this picture:

- Stability boundaries meet transversally at odd resonances and quadratically at even resonances.
- Instability boundaries meeting at the nth resonance have n intersections, counting multiplicity, thereby enclosing the instability pockets. This occurs because the antiprojection line of the nth resonance has exactly n intersection points with S, counting multiplicity.
- This property persists under L^p-small reversible perturbations of Hill's equation. The transversal intersections mentioned above persist, while the quadratic ones are contained in a family of Whitney folds of Section 3.

2. Symplectic reversible matrics

Let us consider Hill's equation

$$\ddot{x} + q(t)x = 0, \quad q(t) \equiv q(t + 2\pi) \tag{2}$$

which is equivalent to the time-periodic linear system

$$\dot{z} = Q(t)z, \tag{3}$$

where

$$z := \begin{pmatrix} x \\ \dot{x} \end{pmatrix}, \quad Q := \begin{pmatrix} 0 & 1 \\ -q & 0 \end{pmatrix}.$$

Let us denote the Poincaré, or period, map of system (3) by P: $z|_{t=0} \mapsto z|_{t=2\pi}$. We recall that P belongs to the symplectic group $Sp(1)$ of 2×2 matrices with $\det P = 1$; see [4].

It is well-known that the symplectic group $Sp(1)$ topologically is an open, solid torus; see GELFAND & LIDSKII [8]. There are several ways to prove this. One method, following [8], is to use a polar decomposition $P = OH$ into the orthogonal

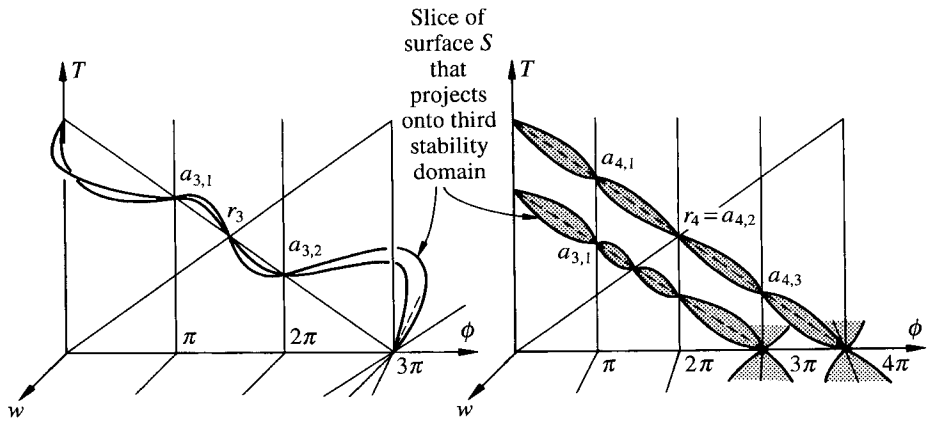

Figure 2. The surface S associated with Hill's equation when p is a square wave. Shaded parts of S in the right-hand figure project onto domains of unstable matrices.

and the symmetric factors, and to observe that the former form a circle while the latter form a disk.

An alternative way to see that $Sp(1) \cong \mathbf{S}^1 \times \mathbf{R}^2$ is to write

$$P = \begin{pmatrix} u + z & v + w \\ -v + w & u - z \end{pmatrix},$$

and to observe that $\det P = 1$ amounts to

$$u^2 + v^2 = 1 + w^2 + z^2. \tag{4}$$

The last equation describes a hyperboloid in $\mathbf{R}^4$ diffeomorphic to $\mathbf{S}^1 \times \mathbf{R}^2$, i.e., an open solid torus. The stable matrices, i.e., the ones with eigenvalues in $\mathbf{S}^1 \setminus \{-1, +1\}$, are characterized by $|\operatorname{tr} P| < 2$ and therefore by $|u| < 1$. The corresponding regions are indicated in Figure 3.

The following well-known proposition is simple to check.

Proposition 2 (Reversible symplectic matrices). *If $q(-t) \equiv q(t)$, the system is reversible, i.e., its Poincaré map satisfies $PRP = R$, where $R = \operatorname{diag}(1, -1)$. In the form* (4) *this is equivalent to $z = 0$, giving the characterization*

$$P = \begin{pmatrix} u & v + w \\ -v + w & u \end{pmatrix}, \quad u^2 + v^2 = 1 + w^2. \tag{5}$$

From now on, by $SR(1)$ we denote the space of reversible symplectic 2×2-matrices. $SR(1)$ is parametrized by vectors (u, v, w) satisfying the equation in (5) constituting a 1-sheeted hyperboloid; see Figure 3. We define the polar angle $\varphi = \arg(u + iv)$ on the covering plane $\widetilde{SR(1)}$. The stability boundaries $|u| = 1$ in $\widetilde{SR(1)}$ correspond to the curves $w = \pm \tan(\varphi - k\pi)$, $k = 1, 2, \ldots$.

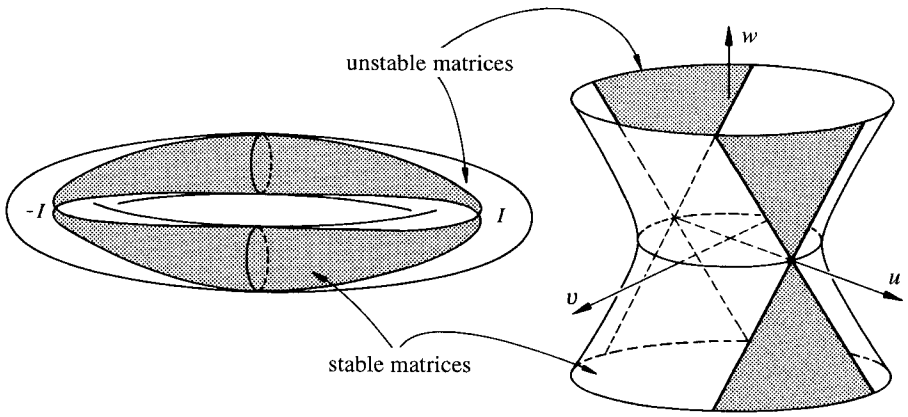

Figure 3. Geometry of the symplectic group and of its reversible subset.

Remark. If $q_b(t) \equiv q_{-b}(t - c)$, for some constant c, where b is a parameter, then the Poincaré matrices P_b and P_{-b} are similar, and thus share stability properties.

As an application of this remark for the equation

$$\ddot{x} + (a + b\cos t + \varepsilon\cos 2t)x = 0,$$

the stability diagram in the (a, b)-plane for any fixed ε is symmetric under reflections in the a-axis. Notice that $\varepsilon = 0$ is the classical Mathieu case.

3. Local creation of an instability pocket by folding

3.1. A reversible perturbation of Mathieu's equation

We study the structure of Hill's map in the reversible perturbation of Mathieu's equation:

$$\ddot{x} + (a + b(\cos t + \varepsilon\cos 2t))x = 0. \tag{6}$$

Near the first resonance $(a, b) = (\frac{1}{4}, 0)$, the situation is qualitatively as in the Mathieu case: the stability boundaries meet transversally. The first interesting case arises near the second resonance $(a, b) = (1, 0)$; for stability diagrams cf. Figure 4. Here H_0 turns out to have a fold (see Figure 5) where the ε-dependence of H_ε is sketched as well. A detailed description of H_ε is given below.

Theorem 3 (Hill's map near second resonance). *Hill's map H_ε of* (6) *in the coordinates* (φ, w) *on* $\widetilde{SR(1)}$ *is given by*

$$\begin{aligned} \varphi &= -\mu_1 + \tfrac{1}{2}\mu_1^2 + c(\varepsilon)\mu_2^2 + O(|\mu|^3), \quad c(\varepsilon) = \tfrac{1}{3} + \tfrac{1}{16}\varepsilon^2, \\ w &= -\tfrac{1}{2}\varepsilon\mu_2 - \tfrac{1}{4}\mu_1\mu_2 + \tfrac{1}{2}\mu_2^2 + O(|\mu|^3), \end{aligned} \tag{7}$$

where $(\mu_1, \mu_2) = \frac{1}{2}((a, b) - (1, 0))$.

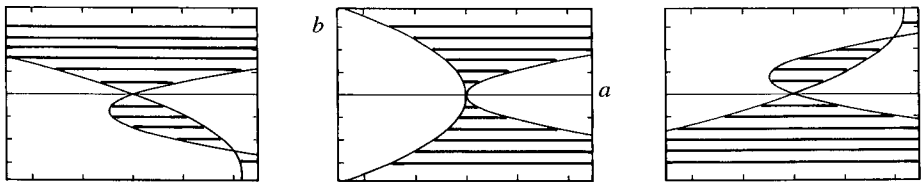

Figure 4. Stability diagrams of a reversible perturbation of Mathieu's equation near the second resonance as ε passes through zero.

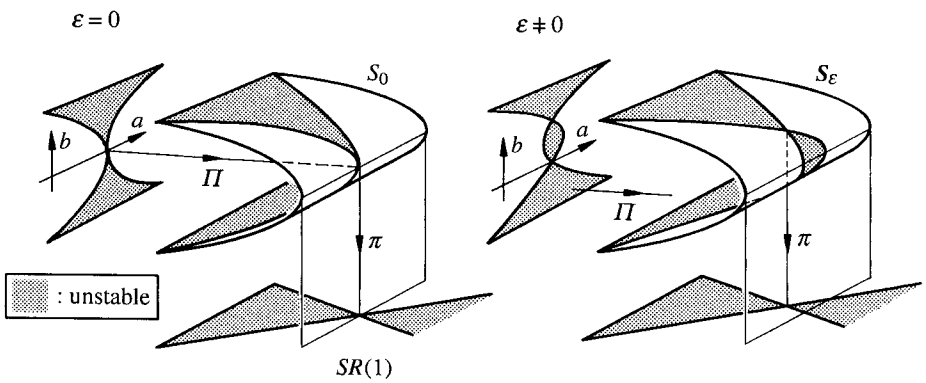

Figure 5. Creation of an instability pocket by folding.

Here and elsewhere the O-estimates are uniform in ε, for ε in a sufficiently small neighborhood of 0. This theorem implies the geometry of Figure 3.

Corollary 4 (Asymptotic description near second resonance).
1. *For $\varepsilon = 0$ the stability boundaries at $(a, b) = (1, 0)$ have a nondegenerate tangency.*
2. *For $\varepsilon \neq 0$ the stability boundaries have two transversal intersections and an instability pocket.*
3. *The stability boundaries at $(a, b) = (1, 0)$ are given by*

$$\begin{aligned} a &= 1 - \tfrac{1}{2}\varepsilon b + (\tfrac{5}{12} - \tfrac{1}{32}\varepsilon^2)b^2 + O(b^3), \\ a &= 1 + \tfrac{1}{2}\varepsilon b - (\tfrac{1}{12} - \tfrac{1}{8}\varepsilon^2)b^2 + O(b^3). \end{aligned} \tag{8}$$

4. *The fold line of H_ε near $(a, b) = (1, 0)$ is given by*

$$b = \varepsilon - \varepsilon(a - 1) + O((a - 1)^2). \tag{9}$$

Proof. We prove the statements of both theorem and corollary by analyzing the local behavior of our 1-parameter family of Hill's maps

$$H_\varepsilon\colon (a, b) \in \mathscr{R}^2 \mapsto P_{a,b;\varepsilon} \in SR(1).$$

Consider the time-dependent Hamiltonian of (6), given by

$$F_\varepsilon(x, y, t; a, b) = \tfrac{1}{2}y^2 + \tfrac{1}{2}(a + b(\cos t + \varepsilon \cos 2t))x^2.$$

By a repeated averaging process, one can obtain an almost autonomous, reversible normal form

$$F_\varepsilon(x, y, t; \mu) = \tfrac{1}{2}E_\varepsilon(\mu)(x^2 + y^2) + \tfrac{1}{2}b\Phi_\varepsilon(\mu)(y^2 - x^2) + O(|\mu|^\infty)$$

for this. Here $\mu = (a - 1, b)$. For details see BROER & VEGTER [7]. We define the corresponding system matrix in $sp(1)$ by

$$L_\varepsilon(\mu) = E_\varepsilon(\mu)\begin{pmatrix} 0 & 1 \\ -1 & 0 \end{pmatrix} + b\Phi_\varepsilon(\mu)\begin{pmatrix} 0 & 1 \\ 1 & 0 \end{pmatrix}; \tag{10}$$

then Hill's map $H_\varepsilon(\mu)$ is given by $H_\varepsilon(\mu) = \exp 2\pi L_\varepsilon(\mu) + O(|\mu|^\infty)$. Again by [7] we have

$$\begin{aligned} E_\varepsilon(\mu) &= \tfrac{1}{2}(a - 1) - \tfrac{1}{8}(a - 1)^2 - \tfrac{1}{4}(\tfrac{1}{3} + \tfrac{1}{16}\varepsilon^2)b^2 + O(|\mu|^3), \\ \Phi_\varepsilon(\mu) &= -\tfrac{1}{4}\varepsilon + \tfrac{1}{8}\varepsilon(a - 1) + \tfrac{1}{8}b + O(|\mu|^2). \end{aligned} \tag{11}$$

These formulae are obtained by averaging twice.

The exponential map

$$A \mapsto \exp 2\pi A \tag{12}$$

is a local diffeomorphism $sp(1) \to Sp(1)$, near $A = 0$. We use this as a local chart, replacing $\mu \mapsto H_\varepsilon(\mu)$ by its logarithm

$$\mu \in \mathscr{R}^2 \mapsto L_\varepsilon(\mu) \in sp(1).$$

The reversibility condition $PR = RP^{-1}$ (see Proposition 2) translates to its infinitesimal version $LR = -RL$, as can be readily checked. If, in the 3-dimensional vector space $sp(1) = sl(2)$ of trace-zero matrices, we consider the ordered basis

$$\left\{\begin{pmatrix} 0 & 1 \\ -1 & 0 \end{pmatrix}, \begin{pmatrix} 0 & 1 \\ 1 & 0 \end{pmatrix}, \begin{pmatrix} 1 & 0 \\ 0 & -1 \end{pmatrix}\right\},$$

with respective coordinates (ξ, η, ζ), then the space $sr(1)$ of infinitesimally reversible matrices is exactly the plane $\zeta = 0$. Moreover, the domain of stable matrices in $\zeta = 0$ corresponds to $|\xi| \geqq |\eta|$. These statements follow by direct computation.

After these preliminaries, we can express the planar map $\mu \in \mathscr{R}^2 \mapsto L_\varepsilon(\mu) \in sr(1)$ in the coordinates a, b, ξ and η. Indeed, by (10) and (11), this map is given by $\xi = E_\varepsilon(\mu)$, $\eta = b\Phi_\varepsilon(\mu)$, or more explicitly by

$$\begin{aligned} \xi &= \tfrac{1}{2}(a - 1) - \tfrac{1}{8}(a - 1)^2 - \tfrac{1}{4}(\tfrac{1}{3} + \tfrac{1}{16}\varepsilon^2)b^2 + O(|\mu|^3), \\ \eta &= -\tfrac{1}{4}\varepsilon b + \tfrac{1}{8}(a - 1)b + \tfrac{1}{8}b^2 + O(|\mu|^3). \end{aligned} \tag{13}$$

For the Jacobian determinant of (13) we find

$$\frac{\partial(\xi, \eta)}{\partial(a, b)} = -\tfrac{1}{8}\varepsilon + \tfrac{1}{8}\varepsilon(a - 1) + \tfrac{1}{8}b + O(|\mu^2),$$

yielding the fold line (9). Also the stability boundaries, determined by $\xi = \pm\eta$, or equivalently by $E = \pm b\Phi$, are easily seen to have the form (8). Moreover, we compute the L_ε-image of the fold line (9) as given parametrically by

$$\begin{aligned} \xi &= -\tfrac{1}{4}(\tfrac{1}{3} + \tfrac{1}{16}\varepsilon^2)\varepsilon^2 + \tfrac{1}{2}(1 + \varepsilon^2(\tfrac{1}{3} + \tfrac{1}{16}\varepsilon^2))(a-1) + O(|a-1|^2), \\ \eta &= -\tfrac{1}{4}\varepsilon^2 - \tfrac{1}{8}\varepsilon^2(a-1) + O(|a-1|^2). \end{aligned} \tag{14}$$

Finally, we easily check the following (local) relations between the coordinates (ξ, η) in $sr(1)$ and (φ, w) in $\widetilde{SR(1)}$ (see (12)):

$$\begin{aligned} \varphi(\xi, \eta) &= -\xi + O(|(\xi, \eta)|^3), \\ w(\xi, \eta) &= \eta + O(|(\xi, \eta)|^3). \end{aligned}$$

From this the proofs of Theorem 3 and Corollary 4 are straightforward. □

3.2. *A local universal model for the Hill map family H_ε*

To better understand the family H_ε we bring it into a Whitney normal form by changing variables in both range and domain as well as reparametrizing ε. Such a compound transformation is referred to as a left-right equivalence; for example, see [14]. Most importantly this serves to establish the qualitative persistence of Theorem 3 in this Hamiltonian reversible setting. As a background for this kind of approach; for example, see ARNOLD [2].

More formally, two families M_ε and F_ε of maps are left-right equivalent if there exist diffeomorphisms $(\Psi_\varepsilon, \Phi_\varepsilon)$ as well as a reparametrization $\rho(\varepsilon)$ making the following diagram commute.

$$\begin{array}{ccc} (\mathscr{R}^2, 0) & \xrightarrow{F_\varepsilon} & (\mathscr{R}^2, 0) \\ \downarrow{\scriptstyle \Phi_\varepsilon} & & \downarrow{\scriptstyle \Psi_\varepsilon} \\ (\mathscr{R}^2, 0) & \xrightarrow{M_\rho(\varepsilon)} & (\mathscr{R}^2, 0) \end{array}$$

Theorem 5 (A Whitney normal form). *Within the class of all local C^2 1-parameter families of planar maps that fix the origin, there exists a C^2-neighborhood of the family $H_\varepsilon(a, b)$, all elements of which are left-right equivalent to M_ε: $(\xi, \eta) \in (\mathscr{R}^2, 0) \mapsto (\xi, \eta^2 - 2\varepsilon\eta) \in (\mathscr{R}^2, 0)$. Under this equivalence, stability boundaries transform into curves transversal to the image of the fold line.*

Proof. By quadratic left-right equivalence we can bring the lower-order terms of (7) into the form M_ε. The following geometric properties of (7) enable us to do this.

1. Both the fold line and its image are tangent to the horizontal axis, while the stability boundaries have a nondegenerate (quadratic) tangency.
2. The fold line, as a function of ε, moves with positive speed.

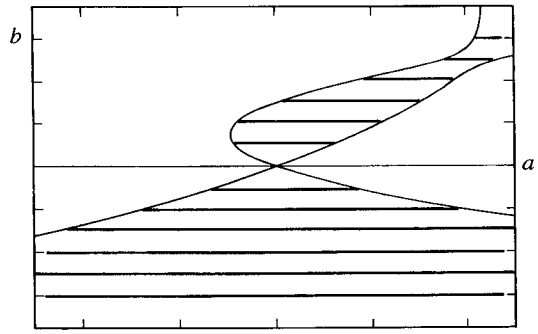

Figure 6. Opening of an instability pocket under non-reversible perturbation of Mathieu's equation near the second resonance.

Moreover, the transversality of the stability boundaries to the image of the fold line turns out to be preserved under this equivalence. By a parameter-dependent version of Whitney's theorem (cf. BRÖCKER & LANDER [14]), the higher-order terms can be removed. Since the properties 1 and 2 are C^2-open, the family H_ε is structurally stable under left-right equivalence with normal form in M_ε. □

In Figure 5, we show the decomposition $H_\varepsilon = \pi \circ \Pi_\varepsilon$. The surface $S_\varepsilon \subset \mathscr{R}^3$ is given by the parametrization Π_ε: $(\xi, \eta) \mapsto (\xi, \eta, \eta^2 - 2\varepsilon\eta)$, while π: $S_\varepsilon \to SR(q)$ projects onto the first two coordinates. For $\varepsilon \neq 0$ the map H_ε folds the parameter plane along a line, doubly covering the half-plane of $SR(1)$ containing I. The image of the fold line consists of the points above which π fails to have maximal rank.

In general such a decomposition of a 2-dimensional map involves its graph, which is a surface in $\mathscr{R}^4$. In the present case, however, this surface can be embedded in $\mathscr{R}^3$.

Remarks. i. It is unclear whether the left equivalences Ψ_ε can be made to respect the 'cross' $\xi = \pm\eta$. The fact that for $\varepsilon = 0$ only three lines through the origin are involved gives some hope for this.

ii. An example with the coefficient function $p(t) = \cos t + \varepsilon_1 \cos 2t + \varepsilon_2 \sin 2t$ perturbs away from the reversible setting. Now the image space is 3-dimensional and folding no longer is generic. For $\varepsilon_2 = 0$ we still are in the above, reversible setting, with the stability diagrams of Figure 4. For $\varepsilon_2 > 0$, however, a corresponding stability diagram is shown in Figure 6.

Here, in the (a, b)-plane we consider the level curves of the 2-parameter family of functions $\Delta_{\varepsilon_1, \varepsilon_2} = \det L_{\varepsilon_1, \varepsilon_2} = E^2_{\varepsilon_1, \varepsilon_2} - b^2 |\Phi_{\varepsilon_1, \varepsilon_2}|^2$. Indeed, the zero level of $\Delta_{\varepsilon_1, \varepsilon_2}$, which always contains the resonance $(a, b) = (1, 0)$, exactly gives the stability boundaries. Instead of (11) we now have

$$E_\varepsilon(\mu) = \tfrac{1}{2}(a-1) - \tfrac{1}{8}(a-1)^2 - \tfrac{1}{4}(\tfrac{1}{3} + \tfrac{1}{16}(\varepsilon_1^2 + \varepsilon_2^2))b^2 + O(|\mu|^3),$$

$$\Phi_\varepsilon(\mu) = -\tfrac{1}{4}\varepsilon_1 + \tfrac{1}{8}\varepsilon_1(a-1) + \tfrac{1}{8}b + i(\tfrac{1}{4}\varepsilon_2 - \tfrac{1}{8}\varepsilon_2(a-1)) + O(|\mu|^2),$$

with Φ complex-valued. Applying singularity theory to this, we find a normal form

$$\Delta_{\kappa,\nu}(\alpha,\beta) = \alpha^2 - \beta^4 + \kappa\beta^3 + \nu\beta^2.$$

Here $\kappa \sim \varepsilon_1 + \varepsilon_2^2$ and $\nu \sim -(\varepsilon_1^2 + \varepsilon_2^2)$, while $\alpha = a - 1 + O(|\mu|^2)$ and $\beta = b$. The origin $(\alpha, \beta) = (0, 0)$ for all parameter values is still a critical point in the zero level set. In the parameter region of interest to us, this is a saddle point. Moreover, the function $\Delta_{\kappa,\nu}$ here has one more saddle point. The point is that the levels of these saddles coincide for $\varepsilon_2 = 0$, while they do not for $\varepsilon_2 \neq 0$. This explains the diagrams shown in Figure 6.

iii. At the third resonance $(a, b) = (\frac{9}{4}, 0)$ the stability boundaries of Mathieu's equation have third order of contact. Here a local analysis of (1) with the 2-parameter deformation $p(t) = \cos t + \varepsilon\cos 2t + \delta\cos 3t$ of coefficient functions is likely to reveal a family of Whitney cusps. A formula manipulator would be helpful here.

4. Geometry in the large of the Hill equation when p is a square wave

In this section we consider the Hill equation

$$\ddot{x} + (a + b\,\mathrm{sgn}\cos t)x = 0, \tag{15}$$

i.e., equation (1) with $p(t) = \mathrm{sgn}\cos t$. Our aim is to describe the global geometric picture of Hill's map H: $(a, b) \mapsto P_{a,b}$. The diagram is symmetric under reflection in the a-axis, by the remark following Proposition 2.

4.1. Geometric picture — a summary

We consider the Hill map H: $\mathbf{R}^2 \to SR(1)$ associated with the Hill equation (15). This map wraps and folds the quadrant

$$Q := \{(a, b) \in \mathbf{R}^2 : a > |b|\} \tag{16}$$

around the cylinder $SR(1)$. This quadrant contains all the interesting parameter values of (15). In order to unwrap its image, we consider a lift $\tilde{H}$ to the covering plane $\widetilde{SR(1)} \cong \mathbf{R}^2$. This lift still fails to be 1 : 1, due to the 'folding' part: In fact, the analysis below shows that it has infinitely many fold lines and has a transcedental nature.

We give a decomposition $H = \pi \circ \Pi$ into a diffeomorphism Π of Q onto a smooth surface $S \subset \mathscr{R}^3$ and a projection π onto the horizontal plane in $\mathscr{R}^3$:

$$\tilde{H}: Q \xrightarrow{\Pi} S \subset \mathscr{R}^3 \xrightarrow{\pi} \widetilde{SR(1)}. \tag{17}$$

Here π is the (skew) projection in the direction $(1, 0, -2)$, as in Figure 7. The surface S and the map Π are specified in Proposition 8 below. Postponing the formulas, we give the geometric corollaries. We show how the properties of the

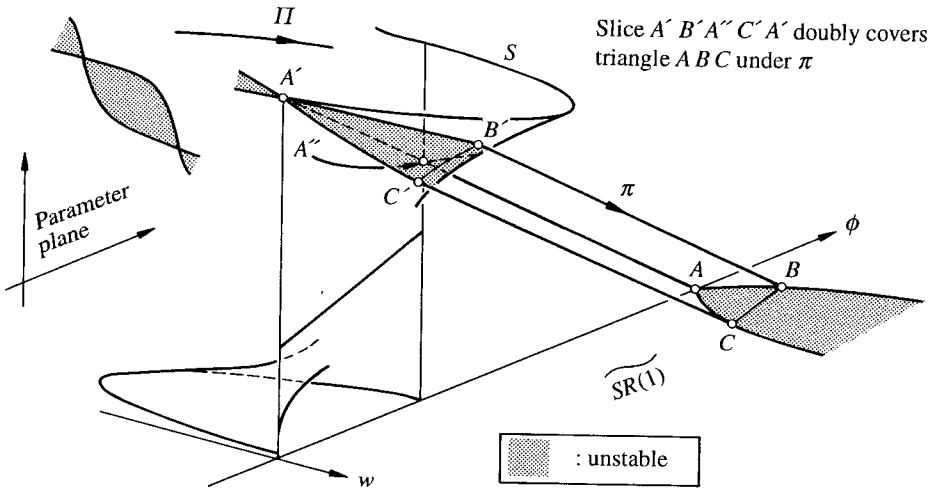

Figure 7. A fundamental piece of the surface S and an instability pocket of Hill's equation where p is a square wave. The shaded part of S projects onto the shaded instability domain in $SR(1)$.

stability diagram mentioned in Section 1 (also, see Figure 1) are encoded in Figures 7 and 2.

Referring to Proposition 2, we see that the point $(\pi \circ \Pi)(a, b) = (\varphi, w)$ gives the coordinates of the image under Hill's map

$$\tilde{H}(a, b) = \begin{pmatrix} u & v + w \\ -v + w & u \end{pmatrix},$$

where u and v satisfy $u^2 + v^2 = 1 + w^2$, and where $\varphi = \arg(u + iv)$. We denote the coordinates in $\mathbf{R}^3 \equiv \widetilde{SR(1)} \times \mathbf{R}$ by (φ, w, T). For any k, let $R_k^{\pm}$ be the ruled surface in $\mathscr{R}^3 = \{(\varphi, w, T)\}$ obtained by π-antiprojection of the stability boundary $w = \pm \tan(\varphi - k\pi)$. Also let $r_k = (\frac{k}{2}\pi, 0, k\pi)$ and $a_{k,m} = (m\pi, 0, 2(k-m)\pi)$, $m = 1, 2, \ldots, k-1$. Note that $r_k = a_{k,1/2k}$ for k even. All this is shown in Figure 2.

Theorem 6 (Geometry of the surface S). *The surface S, which is the image under the diffeomorphism Π: $Q \to S \subset \mathscr{R}^3 = \{(\varphi, w, T)\}$, has the following properties.*

1. *S intersects the plane $w = 0$ along the vertical straight lines $\varphi = m\pi$, $w = 0$, $m = 1, 2, \ldots$, as well as along the straight line $T = 2\varphi$, $w = 0$. These lines intersect at the points r_{2m}: S is everywhere transversal to $w = 0$, except at those points.*
2. *For any fixed $k \in \mathcal{N}$, the intersection $S \cap R_k^{\pm}$ contains a piecewise analytic curve $\partial_k^{\pm}$. The two curves ∂_k^{+} and ∂_k^{-} intersect at $a_{k,m}$, $m = 1, 2, \ldots, k-1$, and at r_k.*
3. *The projection π from S is a diffeomorphism near r_n for n odd and has a fold at r_n for n even. Moreover, the estimates of* Arnold [4] *on the sharpness of the*

resonance tongues are recovered:

$$a = \frac{1}{4}n^2 \pm \frac{2}{n\pi}b + o(b) \qquad \textit{for odd } n,$$

$$a = \frac{1}{4}n^2 \pm \frac{4}{n^2}b^2 + o(b^2) \quad \textit{for even } n.$$

A proof is given below. Theorem 6 implies

Corollary 7 (Properties of stability regions in the parameter plane). *The two boundaries of the stability regions which meet at the nth resonance have exactly n points of intersection, counting multiplicity. For n odd, n of these intersections are transversal, yielding n distinct points and at least n + 1 instability pockets. For n even, the two boundary curves have a nondegenerate quadratic tangency at the resonance, while the remaining n − 2 intersections are transversal, yielding at least n instability pockets.*

Remarks. i. The existence of n intersections (counting multiplicity) between the boundaries of the nth instability persists under L^r-small reversible perturbations of Hill's equation with p a square wave.
ii. Under any L^r-small reversible perturbation, the quadratic tangencies at $r_n = a_{n,n/2}$, for even n, are contained in a fold family described in the previous section, in general creating an extra instability pocket.
iii. If the transversality of the two surfaces were shown, it would follow that $\partial_k^{\pm}$ are smooth curves. In that case, the term 'at least' in Corollary 7, concerning the numbers of instability pockets, can be replaced by 'exactly'. Although transversality is not easy to establish analytically, it is strongly suggested by numerical evidence.

4.2. Decomposiiton of Hill's map

The first step of our analysis of (15) is a rescaling of time, with the aim of making the phase flow a Euclidean rotation for half the period. Setting

$$\tau := \frac{T}{2\pi}t,$$

where T is a parameter, turns (15) into

$$x'' + \left(\frac{2\pi}{T}\right)^2 \left(a \pm b \operatorname{sgn} \cos \frac{2\pi}{T}\tau\right) x = 0.$$

We now choose T such that

$$\left(\frac{2\pi}{T}\right)^2 (a + b) = 1 \tag{18}$$

and denote

$$\left(\frac{2\pi}{T}\right)^2 (a-b) =: B. \tag{19}$$

The old parameters a and b have been replaced by B and T, given by (18) and (19), or, more explicitly, by

$$B = \frac{a-b}{a+b}, \quad T = 2\pi\sqrt{a+b}. \tag{20}$$

Renaming τ back to t, we obtain the following equivalent form for Hill's equation (15):

$$\ddot{x} + p(t)x = 0, \quad p(t) = \begin{cases} 1 & \text{if } \cos(2\pi t/T) > 0, \\ B & \text{otherwise.} \end{cases} \tag{21}$$

We take $B > 0$ and $T > 0$, which in the (a, b)-plane gives the restriction to the quadrant $Q = \{(a, b) \in \mathbf{R}^2 : a > |b|\}$. Our goal now is to decompose the transformed Hill map H: $(B, T) \mapsto P_{B,T}$.

Proposition 8. *The lift* $\tilde{H}: Q \to \widetilde{SR(1)} = \{\varphi, w\}$ *is a composition* $\tilde{H} = \Pi \circ \pi$. *The diffeomorphism* Π *is given by*

$$(B, T) \mapsto (\varphi, w, T),$$

where

$$u = \cos\sqrt{B}\frac{T}{2}, \quad v = \frac{1}{2}\left(\sqrt{B} + \frac{1}{\sqrt{B}}\right)\sin\sqrt{B}\frac{T}{2}, \quad w = \frac{1}{2}\left(\sqrt{} - \frac{1}{\sqrt{B}}\right)\sin\sqrt{B}\frac{T}{2}, \tag{22}$$

and the skew projection π *is given by*

$$(\varphi, w, T) \mapsto \left(\varphi + \frac{T}{2}, w\right). \tag{23}$$

Proof. Since (21) has piecewise-constant coefficients, the Poincaré map P is the composition

$$P = P_1 \circ P_2 \circ P_1, \tag{24}$$

with

$$P_1 = R_{T/4},$$

where

$$R_\alpha = \begin{pmatrix} \cos\alpha & \sin\alpha \\ -\sin\alpha & \cos\alpha \end{pmatrix}, \quad P_2 = \begin{pmatrix} \cos\sqrt{B}\frac{T}{2} & \frac{1}{\sqrt{B}}\sin\sqrt{B}\frac{T}{2} \\ -\sqrt{B}\sin\sqrt{B}\frac{T}{2} & \cos\sqrt{B}\frac{T}{2} \end{pmatrix}.$$

Writing P_2 in the coordinates (u, v, w) of (5) gives (22).

To compute the product (24), we observe a simple but important relation: If

$$\begin{pmatrix} U & V+W \\ -V+W & U \end{pmatrix} = R_\alpha \begin{pmatrix} u & v+w \\ -v+w & u \end{pmatrix} R_\alpha, \tag{25}$$

then

$$\begin{pmatrix} U \\ V \end{pmatrix} = R_{2\alpha} \begin{pmatrix} u \\ v \end{pmatrix}, \quad W = w. \tag{26}$$

Applying this remark to (24) we conclude that the (U, V, W)-coordinates of P are given by (26) with $2\alpha = T/2$ such that $\arg(U + iV) = \varphi + T/2$. This proves (23). □

4.3. *Proofs of Theorem 6 and Corollary 7*

Theorem 6.1 follows immediately from Proposition 8. We first sketch a proof of Theorem 6.2, showing the existence of a boundary curve $\partial^+_{k,m} \subset S_m \cap R^+_k$, where $S_m = S \cap \{(m-1)\pi \leqq \varphi \leqq m\pi\}$, $1 \leqq m \leqq k$.

Consider the piece of S_m given by

$$\frac{1}{L} \leqq B \leqq L, \quad L \text{ large}, (m-1)\pi \leqq \frac{\sqrt{B}T}{2} \leqq m\pi,$$

which is a topological rectangle parametrized by B, $\theta = \sqrt{B}T/2$. The top boundary, given by $B = L$, lies above the surface R^+_k, while the lower boundary, given by $B = L^{-1}$, lies below R^+_k. Hence the scalar function $f(B, \theta) = \text{proj}_T(\Pi(B, T) - R^+_k(B, T))$, where $T = 2\theta/\sqrt{B}$ and where $R^+_k(B, T)$ is the point on R^+_k on the same vertical as $\Pi(B, T)$, has values of opposite signs on the two opposite sides of the rectangle. Together with the analyticity of f this implies that the zero level set of f contains a piecewise-analytic curve $\partial^+_{k,m}$. In fact $\partial^+_{k,m}$ connects the points $a_{k,m-1}$ and $a_{k,m}$, since these are the only zeros of f on the boundary of the rectangle. We define $\partial^+_k = \bigcup_{m=1}^k \partial^+_{k,m}$. Since S meets $R^\pm_k$ precisely at r_k and at the $a_{k,m}$, $m = 1, 2, \ldots, k-1$, we conclude that the curves $\partial^\pm_k$ also meet precisely at these points.

It remains to prove Theorem 6.3, and in particular to give a geometric explanation of the 'sharpness' of the resonance tongues. Let us start with the odd resonances $a = (k + \frac{1}{2})^2$, $b = 0$, $k = 1, 2, \ldots$. The stability boundaries are the preimages of two curves in $\widetilde{SR(1)}$, the tangent lines of which at $\varphi = (2k+1)\pi$, $w = 0$ are given by $dw = \pm d\varphi$. Computing their preimage under the linearization of $\tilde{H}$: $(a, b) \mapsto (\varphi, w)$ we recover ARNOLD's estimate [4] on the stability boundaries at the odd resonances

$$a = (k + \tfrac{1}{2})^2 \pm \frac{1}{\pi(k + \frac{1}{2})} b + o(b).$$

A similar argument explains the quadratic tangencies of the even resonance tongues. We consider the point $r_{2k} = (k\pi, 0, 2k\pi) \in S$, observing that the surface S at this point is vertical. In fact, the tangent plane here is given by $w = 0$, causing degeneracy of the skew projection π onto the (φ, w)-plane. A simple calculation shows that S is given locally by

$$dw = \tfrac{1}{2}(-1)^k(k\pi dB^2 + dB\,dT), \quad d\varphi = \tfrac{1}{2}k\pi dB + dT,$$

or equivalently in terms of (a, b),

$$dw = \frac{\pi}{k^3}(-1)^{k+1}(da\,db - db^2), \quad d\varphi = \frac{\pi}{k}da.$$

This shows that S is a saddle near r_{2k}, which projects by π as a fold.

As before, the stability boundaries meeting at $a = k^2, b = 0$ are the preimages of the two boundaries $w = \pm \tan(\varphi - 2k\pi)$ with tangents $dw = \pm d\varphi$ at the resonances $\varphi = 2k\pi$, $w = 0$. This leads to the infinitesimal equation

$$da = \pm \frac{1}{k^2}db^2 + o(db^2),$$

and hence to

$$a = k^2 \pm \frac{1}{k^2}b^2 + o(b^2).$$

Acknowledgements. We thank FLORIS TAKENS & GERT VEGTER for stimulating discussion and WARREN WECKESSER for computing Figures 1, 4 and 6. This research was supported by the Netherlands Organization of Scientific Research (N.W.O.). LEVI gratefully acknowledges support by the Air Force Office of Scientific Research.

References

1. Z. AFSHARNEJAD. Bifurcation geometry of Mathieu's equation. *Indian J. Pure Appl. Math.* **17** (1986), 1284–1308.
2. V. I. ARNOLD. Lectures on bifurcations in versal families. *Russ. Math. Surv.* **27** (1972), 54–123.
3. V. I. ARNOLD. Loss of stability of self-oscillation close to resonance and versal deformations of equivariant vector fields. *Funct. Anal. Appl.* **11** (1977), 85–92.
4. V. I. ARNOLD. *Mathematical Methods of Classical Mechanics*, Springer-Verlag, 1980.
5. V. I. ARNOLD. *Geometrical Methods in the Theory of Ordinary Differential Equations.* Springer-Verlag, 1983.
6. V. I. ARNOLD. Remarks on the perturbation theory for problems of Mathieu type. *Russ. Math. Surv.* **38** (1983), 215–233.
7. H. W. BROER & G. VEGTER. Bifurcational aspects of parametric resonance. *Dynamics Reported, New Series* **1** (1992), 1–53.
8. I. M. GELFAND & V. B. LIDSKII. On the structure of stability of linear canonical systems of differential equations with periodic coefficients. *Amer. Math. Soc. Transl.* (2) **8** (1958), 143–181.

9. J. PÖSCHEL & E. TRUBOWITZ. *Inverse Spectral Theory*. Academic Press, 1986.
10. M. LEVI. Stability of the inverted pendulum – a topological explanation. *SIAM Review* **30** (1988), 639–644.
11. D. M. LEVY & J. B. KELLER. Instability intervals of Hill's equation. *Comm. Pure Appl. Math.* **16** (1963), 469–479.
12. J. MEIXNER & F. W. SCHÄFKE. *Mathieusche Funktionen und Sphäroidfunktionen*. Springer-Verlag, 1954.
13. J. J. STOKER. *Nonlinear Vibrations*. Interscience, 1950.
14. TH. BRÖCKER & L. LANDER. *Differentiable Germs and Catastrophes*. Cambridge University Press, 1976.
15. B. VAN DER POL & M. J. O. STRUTT. On the stability of the solutions of Mathieu's equation. *The London, Edinburgh and Dublin Phil. Mag. 7th Series* **5** (1928), 18–38.
16. M. I. WEINSTEIN & J. B. KELLER. Hill's equation with a large potential. *SIAM J. Appl. Math.* **45** (1985), 954–958.
17. M. I. WEINSTEIN & J. B. KELLER. Asymptotic behavior of stability regions for Hill's equation. *SIAM J. Appl. Math.* **47** (1987), 941–958.

Department of Mathematics
University of Groningen
PO Box 800
9700 AV Groningen, The Netherlands

and

Department of Mathematical Sciences
Rensselaer Polytechnic Institute
Troy, New York 12180

(Accepted October 21, 1994)